Electrical Power and Energy Systems 155 (2024) 109499

Contents lists available at ScienceDirect

International Journal of Electrical Power and Energy Systems

journal homepage: www.elsevier.com/locate/ijepes

Chance-constrained multi-stage stochastic energy system expansion planning with demand satisfaction flexibility

Yuang Chen [a,b,*], Beste Basciftci [c], Valerie M. Thomas [b]

[a] Georgia Tech Shenzhen Institute, Tianjin University, Shenzhen, China
[b] H. Milton Stewart School of Industrial and Systems Engineering, Georgia Institute of Technology, Atlanta, GA, 30332, USA
[c] Department of Business Analytics, Tippie College of Business, University of Iowa, Iowa City, IA, 52242, USA

ARTICLE INFO

Keywords:
Energy system expansion planning (ESEP)
Multi-stage stochastic optimization
Power deficit flexibility
Chance constraints
Progressive hedging algorithm (PHA)
Sub-saharan africa

ABSTRACT

A classic multi-period stochastic energy system expansion planning (ESEP) model aims to address demand uncertainty by requiring immediate demand satisfaction for all scenarios. However, this approach may result in an expensive system that deviates from the planner's long-term goals, especially when facing unexpectedly high demand scenarios. To address this issue, we propose a chance-constrained stochastic multi-stage ESEP model that allows for a portion of demand to remain unmet in specific periods while still ensuring complete demand satisfaction during most of the planning horizon, including the final period. This approach provides more time flexibility to build infrastructure and assess needs, ultimately reducing costs and allowing for a broader view of infrastructure planning options. To solve the chance-constrained stochastic model, we introduce a binary-search-based progressive hedging algorithm heuristic, which is particularly useful for large-scale models. We demonstrate the effectiveness and benefits of implementing the chance-constrained model through a case study of Rwanda using real-world data.

1. Introduction

There are multiple social and economic benefits from expanding energy systems and improving energy access [1]. Yet building new energy systems is often constrained by physical resources, budgets, and environmental concerns [2]. Overcoming these challenges in a timely manner can be difficult for energy system planners, especially when demand is uncertain.

While future electricity demand is often estimated by extrapolating from the past, there are many examples of unexpectedly high demand [3]. In Kenya, low investment in electricity infrastructure has led to ongoing rolling blackouts [4] even while consumer demand was less than projected [5]. In the United States and Europe, heat waves are driving power consumption to historic levels. The desire to reach sustainable development goals brings forward the complex relationship between economic development and energy demand [6]. An energy system expansion planning (ESEP) model that acknowledges and explicitly incorporates future demand uncertainty [7] can provides strategic planning perspective.

The ESEP problem under demand uncertainty is generally solved within a stochastic optimization framework [8]. In two-stage stochastic optimization, all investment decisions are made in the first stage and operational decisions are made in the second stage to match conditions at that time. In contrast, multi-stage stochastic optimization lets both investment and operational decisions adapt to conditions at each planning period [9]. This more flexible structure may result in a more cost-effective solution, although requiring additional computation.

Demand satisfaction in the standard ESEP problem requires the planner to satisfy all demands at each planning period [10]. Ensuring the capability to satisfy all demands at each time, particularly those that are least probable and large, has drawbacks. First, this requirement may result in a more expensive power infrastructure network. This infrastructure may not be as desirable as what could be developed with a more patient approach. To satisfy an unexpectedly large demand, the model may prioritize building localized power generators instead of constructing sufficient transmission lines due to time constraints. This short-term decision-making may result in a less desirable system compared to those with a more extensive transmission network. One possible solution is the implementation of demand response during the ESEP process. However, traditional demand response mechanisms originate from the end user's side, and the demand curtailment is typically implemented without considering the probability of future demand being either high or low.

* Corresponding author at: Georgia Tech Shenzhen Institute, Tianjin University, Shenzhen, China.
E-mail address: yuang.chen@gatech.edu (Y. Chen).

https://doi.org/10.1016/j.ijepes.2023.109499
Received 27 December 2022; Received in revised form 29 June 2023; Accepted 10 September 2023
Available online 27 September 2023

Nomenclature

Sets and Related Indices

$\mathcal{T}$	Set of time periods (years), indexed by t
Ω	Set of scenarios, indexed by ω
Ω_t	Set of scenarios for indistinguishable state variables at year t, indexed by ω
Φ_G	Set of generation technology types, indexed by g
K	Set of transmission line types, indexed by k
$L^+/L^E/L$	Set of (potential/existing/all) transmission lines, indexed by ij denoting transmission line from region i to region j
N	Set of geographical regions, indexed by i
O	Set of representative daily sub-periods, indexed by o

Parameters

α_t	Chance constraint risk parameter [%]
$\bar{\theta}$	Maximum value of voltage angles [radians]
η_i^{dist}	Distribution efficiency in region i [%]
γ	Discount rate [%]
μ_{ij}^{trans}	Loss of transmission in electricity between regions i and j [%]
π_ω	Probability associated with scenario ω
BUD_t	Investment budget at year t [$]
$B_{ij,k}$	Susceptance of type k transmission line between region i and j [simens]
$c_{g,t}^{\text{fuel-C}}$	Fuel cost of generation type g at time period t per unit generated [$/MWh]
$c_g^{\text{fom-G}}$	Annual fixed O&M cost of generation type g per unit installed [$/MW]
$c_g^{\text{inv-G}}$	Investment cost of generation type g per unit installed [$/MW]
$c_g^{\text{vom-G}}$	Variable O&M cost of generation type g per unit generated [$/MWh]
$c_k^{\text{fom-L}}$	Annual fixed O&M cost of type k transmission line per unit distance [$/km]
$c_k^{\text{inv-L}}$	Investment cost of potential type k transmission line per unit distance [$/km]
$CF_{g,o}$	Capacity factor of generation type g on daily sub-period o [%]
$D_{i,t,o,\omega}$	Electricity demand in region i at year t on daily sub-period o under scenario ω [MWh]
d_{ij}	Distance between region i and region j [km]
$F_k^{\max}$	Max capacity of type k transmission line
GHG_t^{max}	Maximum allowed GHG emission at year t [tons]
GHG_g	GHG emission for generation type g per unit generated [tons/MWh]
h_o	Total hours of daily sub-period o in a year [h]
k_{ij}	Type of the existing transmission line ij
$Q_g^{\min}/Q_g^{\max}$	Annual minimal/maximum investment capacity limit for generation type g [MW]
$Q_{i,g}^{\text{ex}}$	Existing capacity of generation type g in region i [MW]
$R_{i,g}$	Resource limit of generation type g in region i [MW]
RR^{res}	Required percentage of demand for electricity reserve [%]
t_0	Initial year
T_g^G/T_k^L	Construction time for generation type g/type k transmission line [years]

Decision Variables

$\theta_{i,t,o,\omega}$	Voltage angle in region i at year t on daily sub-period o under scenario ω [radians]
$E_{i,g,t,o,\omega}^{\text{gen}}$	Electricity generation of generation type g in region i at year t on daily sub-period o under scenario ω [MWh]
$E_{i,g,t,o,\omega}^{\text{res}}$	Electricity reserve from generation type g in region i at year t on daily sub-period o under scenario ω [MWh]
$E_{i,t,o,\omega}^{\text{use}}$	Electricity used in region i at year t on daily sub-period o under scenario ω [MWh]
$E_{ij,t,o,\omega}^{\text{trans}}$	Electricity flow through transmission line ij at year t on daily sub-period o under scenario ω [MWh]
$l_{ij,k,t,\omega}$	Binary variable that decides the investment of potential transmission line ij, which is equal to 1 if a type k transmission line starts construction on ij at year t under scenario ω and 0 otherwise {0,1}
$p_{ij,k,t,o,\omega}^{\text{trans}}$	Power flow on type k transmission line ij at year t on daily sub-period o under scenario ω [MW]
$Q_{i,g,t,\omega}^{\text{new}}/Q_{i,g,t,\omega}^{\text{total}}$	Newly invested/total capacity of generation type g in region i at year t under scenario ω [MW]
$z_{ij,k,t,\omega}$	Binary variable that decides the condition of transmission lines, which is equal to 1 if a type k transmission line is built on line ij at year t under scenario ω and 0 otherwise {0,1}

We propose chance constraints to allow time-flexible demand satisfaction in the multi-stage stochastic ESEP problem. Our objective is to allow the central planner to delay meeting demand in the event of unexpectedly high demand scenarios, with the aim of achieving a more cost-effective energy system. From a narrow modeling perspective, in which the decision maker strictly implements the model decisions, the inclusion of chance constraints offers the decision maker with cost savings at times when the demand is unexpectedly high. However, it is important to acknowledge that decision makers are not obligated to follow the model decisions in a broader context. If an inflexible model requires immediate demand satisfaction through fast construction of new infrastructure, decision makers may abandon the model. From this perspective, chance constraints offer the flexibility that real decision makers may prefer, making the chance-constrained model a more realistic forecast of the cost of energy system expansion. Stochastic optimization plans in the face of uncertainty while chance constraints reduce costs of responding to the unexpected.

We first formulate a multi-stage stochastic optimization model under operational constraints and policy limitations. Then we introduce chance constraints to the demand satisfaction constraint, while still ensuring that demand is satisfied for all scenarios at the end of the planning horizon. We provide a scenario-based mixed integer linear program reformulation of the chance constraints and develop a binary-search-based progressive hedging algorithm (PHA) heuristic for solving the resulting stochastic program efficiently. Finally, we present a case study for the country of Rwanda to highlight the effect of the framework for generation and transmission investment.

There are many uncertainties during the ESEP process. To formulate a general approach and illustrate its application, this paper develops

a case study for a single source of uncertainty: future demand. The chance-constrained model developed in this paper can be extended to ensure or relax other specifications of the ESEP problem in the context of multiple sources of uncertainty.

The remainder of the paper is organized as follows. Section 2 provides a literature review and identifies the contributions of our paper. Section 3 presents the model description and the mathematical formulation of the multi-stage stochastic ESEP model. Section 4 proposes chance constraints that are applied to the demand satisfaction constraints. Section 5 introduces a variant of the progressive hedging algorithm and proposes a heuristic to solve the problem efficiently. Section 6 presents the data and analyses for the Rwanda case study and Section 7 discusses the results. Section 8 concludes the paper with final remarks.

2. Literature review and our contributions

Optimization is widely used for the ESEP problem [8]. Go et al. [11] used co-optimization for generation and transmission expansion planning (G&TEP) under high renewable standards. Bi-level optimization approaches have also been proposed to coordinate the G&TEP problem in a market environment [12]. To address future uncertainty in the ESEP process, approaches including robust [13], two-stage stochastic, and multi-stage stochastic optimization have been studied [14]. Robust optimization, meeting all future possibilities, may overbuild. Two-stage models have fixed investment policies but lack flexibility in infrastructure choices. Multi-stage stochastic optimization can adjust investment decisions over time [15]. For instance, multi-stage stochastic models have been designed to incorporate random power outages, load forecasts, and wind power output fluctuations [16].

In addition to focusing on power system planners, researchers have also investigated ESEP from a national decision maker's aspect. Guerra et al. [17] considered ESEP to find the most cost-effective plan with GHG emission mitigation for Colombia. A similar ESEP model was proposed by Georgiou [18] for the Greek power system. Guo et al. [19] proposed an ESEP model with targeted GHG emission reductions for China. Ionannou et al. [20] used a multi-stage stochastic optimization model for the Indonesian power system considering three uncertainties: demand, renewable technology cost, and traditional fuel price. Multi-stage stochastic models have been utilized to optimize electrification planning for African countries, demonstrating cost savings compared to two-stage models [21]. All previous models required demand to be met in each time period.

Chance constraint is a technique to reduce the risk from uncertainty in stochastic optimization. Chance-constrained stochastic optimization introduces probabilistic constraints, ensuring that the probability of meeting certain requirements is above a threshold value [22]. Huang et al. [23] developed a multi-period ESEP model and applied chance constraints to electricity demand satisfaction constraints. The modeled did not consider future demand realizations. Zhou et al. [24] proposed a two-stage stochastic chance-constrained ESEP problem for British Columbia, although also without adaptability to future demand realizations. Hence, a multi-stage stochastic model that employs the benefits of chance constraints for step by step infrastructure planning has yet to be developed.

Multi-stage stochastic optimization becomes challenging when it involves integer variables and a large number of stages and scenarios [25]. The Progressive Hedging Algorithm (PHA) is useful for such problems, decomposing scenarios by incorporating non-anticipativity constraints into a Lagrangian penalty function [26]. PHA has been successfully applied in various applications such as hydrothermal system expansion planning [27], healthcare operating room assignment [28], and relief distribution with mixed-integer variables [29]. Our chance-constrained multi-stage stochastic optimization problem cannot be solved directly by PHA because the scenarios are linked through these probabilistic constraints. To overcome this challenge, we propose a solution algorithm which integrates PHA with a binary search method.

Summarizing the literature, while stochastic optimization is commonly utilized in the ESEP problem, the requirement for immediate demand satisfaction can be overly restrictive. There is a risk of constructing quick-to-build and higher-cost infrastructures to meet unexpectedly high-demand. A chance-constrained multi-stage stochastic model can reduce these types of risk. Algorithms such as PHA are not suitable for solving large-scale chance-constrained models; an effective heuristic approach is required.

Our work makes the following contributions to the country-level ESEP problem:

- A chance-constrained multi-stage stochastic ESEP model is proposed, which adapts to future demand uncertainty while ensuring full demand satisfaction at the end of the planning horizon.
- A binary-search-based progressive hedging algorithm is designed as a heuristic to reduce the burden of solving the problem with the chance constraints when the number of scenarios is large.
- A case study of Rwanda shows the benefits of the proposed model with cost reductions, potential transmission infrastructure improvement, and lower-cost GHG emission reduction.

3. Multi-stage stochastic ESEP model

We introduce the multi-stage stochastic ESEP model for countries to determine their investment plans under future electricity demand uncertainty. The model guarantees the feasibility of the energy system by considering certain operational constraints. The electricity demand is represented in two time scales: multi-year and representative daily sub-period. The daily sub-periods capture the variations of both electricity demand and solar power availability.

3.1. Scenario tree structure

We use a scenario tree structure to represent the uncertainty of future demand. A scenario tree represents uncertainty as pathways from the initial time to the final time period. Fig. 1 summarizes the scenario tree structure over an example setting; each node corresponds to a realization of uncertainty. A stage denotes a time interval that consists of multiple time periods (years). Several nodes are included in each stage to represent these sets of realizations. In every stage, the planner is required to make two types of decisions: investment decisions (diamonds in Fig. 1) and operations decisions (squares in Fig. 1). Investment decisions are state variables which carry information to the end of the planning horizon. Operations decisions are stage variables which are locally decided to adapt to the current demand. Investment decisions are made once at each year while operations decisions are made according to the representative daily sub-periods in each year. A probability is assigned for each branch in a scenario tree, such that the sum of probabilities for all branches in every time interval is equal to 1.

3.2. Multi-stage stochastic ESEP model

Mathematical formulation of the multi-stage stochastic ESEP model is presented in this section. All decisions are year and scenario based, with subscript t and ω respectively. For simplicity, if not mentioned, the range of indices on the right hand side of constraints are the total sets described in Nomenclature (e.g., $i \in N$, $g \in \Phi_G$, $ij \in L$, $k \in K$, $t \in \mathcal{T}$, $o \in O$, and $\omega \in \Omega$).

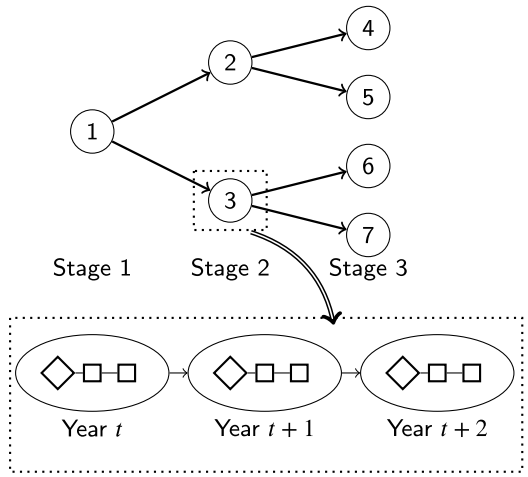

Fig. 1. Scenario tree structure.

3.2.1. Objective

The objective function (1) minimizes the total expected net present cost for all scenarios over all planning periods. For each scenario ω, the net present cost for year t is the total cost at year t multiplied by a discount factor, where γ is an interest rate. The total cost for each scenario at time t has four categories: (i) investment cost, (ii) fixed operations and maintenance (O&M) cost, (iii) variable O&M cost, and (iv) fuel cost. Investment and fixed O&M costs include both power generation capacity and transmission line investments.

$$\begin{aligned}\min \sum_{\omega\in\Omega}\pi_\omega \sum_{t\in\mathcal{T}}\frac{1}{(1+\gamma)^{(t-t_0)}}\cdot\\ \Big[\sum_{i\in N}\sum_{g\in\Phi_G} c_g^{\text{inv-G}} Q_{i,g,t,\omega}^{\text{new}} + \sum_{ij\in L^+}\sum_{k\in K} c_k^{\text{inv-L}} d_{ij} l_{ij,k,t,\omega}\\ + \sum_{i\in N}\sum_{g\in\Phi_G} c_g^{\text{fom-G}} Q_{i,g,t,\omega}^{\text{total}} + \sum_{ij\in L}\sum_{k\in K} c_k^{\text{fom-L}} d_{ij} z_{ij,k,t,\omega}\\ + \sum_{i\in N}\sum_{g\in\Phi_G}\sum_{o\in O} c_g^{\text{VOM-G}}(E_{i,g,t,o,\omega}^{\text{gen}} + E_{i,g,t,o,\omega}^{\text{res}})\\ + \sum_{i\in N}\sum_{g\in\Phi_G}\sum_{o\in O} c_{g,t}^{\text{fuel}}(E_{i,g,t,o,\omega}^{\text{gen}} + E_{i,g,t,o,\omega}^{\text{res}})\Big]\end{aligned} \tag{1}$$

The investment cost includes power and transmission line expansion for all regions. The annual fixed O&M cost depends on the total capacity of the generation and transmission infrastructure. The annual variable O&M cost is the expense for operating and managing power generation plus reserves, excluding fuel costs. The fuel cost for generation and reserves incorporates different fuel costs $c_{g,t}^{\text{fuel}}$ for each year t.

3.2.2. Generation investment and resource limits

Constraint (2) sets annual lower and upper limits for newly invested capacity of each generation type. Constraint (3) defines the total capacity availability for each generation type at each year by considering construction time. Constraint (4) is the resource limitation constraint on the total capacity for each generation technology in each region, bounded by the resource upper limit.

$$Q_g^{\min} \le Q_{i,g,t,\omega}^{\text{new}} \le Q_g^{\max}, \quad \forall i,g,t,\omega \tag{2}$$

$$Q_{i,g,t,\omega}^{\text{total}} = \sum_{\tau\le\max\{t_0,t-T_g^G\}} Q_{i,g,\tau,\omega}^{\text{new}} + Q_{i,g}^{\text{ex}}, \quad \forall i,g,t,\omega \tag{3}$$

$$Q_{i,g,t,\omega}^{\text{total}} \le R_{i,g}^{\max}, \quad \forall i,g,t,\omega \tag{4}$$

3.2.3. Transmission line investment constraints

Constraint (5) defines the transmission line investment binary variable $l_{ij,k,t,\omega}$, which is 1 when a type k line is built on potential line ij at year t in scenario ω and 0 otherwise. Constraint (6) guarantees that at most one transmission line can be built between regions through all years. Constraint (7) defines a new binary variable $z_{ij,k,t,\omega}$ to represent the availability of transmission lines including the potential and existing ones. Constraint (8) checks the availability of the potential transmission line by considering the construction time. The availability of existing transmission lines is set to 1 in constraint (9).

$$l_{ij,k,t,\omega} \in \{0,1\}, \quad \forall ij \in L^+, k,t,\omega \tag{5}$$

$$\sum_{k\in K}\sum_{t\in\mathcal{T}} l_{ij,k,t,\omega} \le 1, \quad \forall ij \in L^+, \omega \tag{6}$$

$$z_{ij,k,t,\omega} \in \{0,1\}, \quad \forall ij \in L^+, k,t,\omega \tag{7}$$

$$z_{ij,k,t,\omega} = \sum_{\tau\le\max\{t_0,t-T_k^L\}} l_{ij,k,\tau,\omega}, \quad \forall ij \in L^+, k,t,\omega \tag{8}$$

$$z_{ij,k,t,\omega} = 1, \quad \forall ij \in L^E, k = k_{ij}, t,\omega \tag{9}$$

3.2.4. Electricity balance and generation limit constraints

The electricity balance constraint (10) imposes the balance in each region at all representative daily sub-periods. In particular, the electricity generated within the region plus the electricity delivered into the region should be greater than or equal to the electricity transferred out of the region and the electricity consumed. Rather than adding a constraint that would curtail demand in cases of insufficient supply, the chance constraint proposed in Section 4 addresses unmet demand with greater flexibility and insight. Constraint (11) imposes an upper limit on electricity generation plus reserves.

$$\sum_{g\in\Phi_G} E_{i,g,t,o,\omega}^{\text{gen}} + \sum_{ji\in L} E_{ji,t,o,\omega}^{\text{trans}} \ge \sum_{ij\in L} E_{ij,t,o,\omega}^{\text{trans}} + E_{i,t,o,\omega}^{\text{use}}, \quad \forall i,t,o,\omega \tag{10}$$

$$E_{i,g,t,o,\omega}^{\text{gen}} + E_{i,g,t,o,\omega}^{\text{res}} \le h_o CF_{g,o} Q_{i,g,t,\omega}^{\text{total}}, \quad \forall i,g,t,o,\omega \tag{11}$$

3.2.5. Reserve constraints

The electricity reserve ensures that the energy system is stable under certain emergency situations. Constraint (12) guarantees that the total electricity reserve meets the reserve requirement, represented by a percentage of the total demand for each year t and daily sub-period o. We use a scalar RR^{res} to denote this required percentage. The flexibility in fulfillment of demand addressed in this paper is a strategic decision, providing longer term flexibility, and not involving reliability-decreasing operational tactics.

$$\sum_{i\in N}\sum_{g\in\Phi_G} E_{i,g,t,o,\omega}^{\text{res}} \ge RR^{\text{res}} \sum_i D_{i,t,o,\omega}, \quad \forall t,o,\omega \tag{12}$$

3.2.6. Demand satisfaction constraints

The multi-stage stochastic ESEP model considers the electricity demand is immediately satisfied for each year. Constraint (13) is the demand satisfaction constraint which guarantees the electricity used is greater than the required electricity demand for each region i at year t on daily sub-period o. Section 4 discusses how flexibility can be incorporated with probabilistic constraints.

$$\eta_i^{dist} E_{i,t,o,\omega}^{\text{use}} \ge D_{i,t,o,\omega}, \quad \forall i,t,o,\omega \tag{13}$$

3.2.7. Power flow constraints

DC approximation power flow constraints are used to ensure physical feasibility, based on the differences of voltage angles in connecting regions. Constraints (14) and (15) are for existing lines and constraints (16)–(18) are for potential lines that can be built. The power flow on a transmission line is limited by the capacity of the type of the transmission line built, which is imposed by (14) and (16). The DC power flow constraints are imposed in (15), (17), and (18). The voltage angles are bounded in constraint (19). One voltage angle is fixed to zero as a reference in constraint (20). Constraint (21) imposes the electricity

transmission restriction while considering the loss during electricity transmission.

$$-F_k^{max} \le p^{\text{trans}}_{ij,k,t,o,\omega} \le F_k^{max}, \quad \forall ij \in L^E, k = k_{ij}, t, o, \omega \tag{14}$$

$$p^{\text{trans}}_{ij,k,t,o,\omega} = B_{ij,k}(\theta_{i,t,o,\omega} - \theta_{j,t,o,\omega}), \forall ij \in L^E, k = k_{ij}, t, o, \omega \tag{15}$$

$$z_{ij,k,t,\omega} F_k^{max} \le p^{\text{trans}}_{ij,k,t,o,\omega} \le z_{ij,k,t,\omega} F_k^{max}, \forall ij \in L^+, k, t, o, \omega \tag{16}$$

$$p^{\text{trans}}_{ij,k,t,o,\omega} - B_{ij,k}(\theta_{i,t,o,\omega} - \theta_{j,t,o,\omega}) \ge -(1 - z_{ij,k,t,\omega})\bar{\theta}, \quad \forall ij \in L^+, k, t, o, \omega \tag{17}$$

$$p^{\text{trans}}_{ij,k,t,o,\omega} - B_{ij,k}(\theta_{i,t,o,\omega} - \theta_{j,t,o,\omega}) \le (1 - z_{ij,k,t,\omega})\bar{\theta}, \quad \forall ij \in L^+, k, t, o, \omega \tag{18}$$

$$-\pi \le \theta_{i,t,o,\omega} \le \pi, \quad \forall i, t, o, \omega \tag{19}$$

$$\theta_{n,t,o,\omega} = 0, \quad n = \text{ref node}, \forall t, o, \omega \tag{20}$$

$$E^{\text{trans}}_{ij,t,o,\omega} \le \sum_{k \in K} h_o p^{\text{trans}}_{ij,k,t,o,\omega}(1 - \mu^{\text{trans}}_{ij}), \quad \forall ij \in L, t, o, \omega \tag{21}$$

3.2.8. Policy constraints

Two policies are considered. Constraint (22) imposes an annual investment budget. Constraint (23) imposes an upper bound on annual GHG emissions. Additional policy constraints can be added.

$$\sum_{i \in N} \sum_{g \in \Phi_G} c_g^{\text{inv-G}} Q^{\text{new}}_{i,g,t,\omega} + \sum_{ij \in L^+} \sum_{k \in K} c_k^{\text{inv-L}} d_{ij} l_{ij,k,t,\omega} \le \text{BUD}_t, \ \forall t \tag{22}$$

$$\sum_{i \in N} \sum_{g \in \Phi_G} \sum_{o \in LO} GHG_g E^{\text{gen}}_{i,g,t,o,\omega} \le GHG_t^{\max}, \quad \forall t, \omega \tag{23}$$

3.2.9. Non-anticipativity constraints

Non-anticipativity ensures that investment decisions (state variables) are made only on information revealed up to current stage, and that scenarios with same history are indistinguishable at each stage. For example, in Fig. 2, when the planner realizes she is in node 2 at the second stage, she shall not know which node is coming for the third stage, only that it is either 4 or 5. Constraints (24) and (25) are non-anticipativity constraints for the investment decisions on generation capacity and transmission lines, respectively.

$$l_{ij,k,t,\omega} = l_{ij,k,t,\omega'} \quad \forall (\omega, \omega') \in \Omega_t, ij \in L^+, k, t \tag{24}$$

$$Q^{\text{new-C}}_{i,g,t,\omega} = Q^{\text{new-C}}_{i,g,t,\omega'} \quad \forall (\omega, \omega') \in \Omega_t, i, g, t \tag{25}$$

4. Chance constraints on demand satisfaction

Here we implement chance constraints to ensure the demand satisfaction within a certain reliability level.

4.1. Chance constraint formulation

The chance constraint allows the desired demand to be met from the generation capacities with a probability of at least $1-\alpha_t$ for a subset of time periods $\mathcal{T}_{CC}$, referred as chance-constrained years, where α_t is the chance constraint risk parameter associated with year t. The proposed chance constraint for demand provides flexibility in fulfilling demand in specified years, managing risks from unexpectedly high demand. This chance constraint can be extended to control supply risks such as those related to imported fuels or local energy resources.

The chance constraint is applied to the demand satisfaction constraint. For non-chance-constrained years we keep the same demand satisfaction requirement in constraint (26). For chance-constrained years we require a minimal fraction of the desired demand to be met in constraint (27), where $\text{req}^{\min}$ denotes the minimal percentage requirement. This constraint guarantees satisfying a certain percentage of demand. Constraint (28) states that the probability of the total electricity consumption satisfying the demand is at least $1-\alpha_t$ for the chance-constrained years.

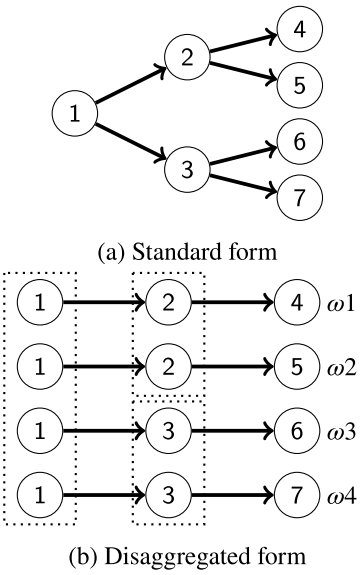

Fig. 2. Scenario tree structure explanation for non-anticipativity constraints.

$$\eta_i^{dist} E^{\text{use}}_{i,t,o,\omega} \ge D_{i,t,o,\omega}, \quad \forall i, t \in \mathcal{T} \setminus \mathcal{T}_{CC}, o, \omega \tag{26}$$

$$\eta_i^{dist} E^{\text{use}}_{i,t,o,\omega} \ge \text{req}^{\min} D_{i,t,o,\omega}, \quad \forall i, t \in \mathcal{T}_{CC}, o, \omega \tag{27}$$

$$Pr(\eta_i^{dist} E^{\text{use}}_{i,t,o,\omega} \ge D_{i,t,o,\omega}, \forall i, o, \omega) \ge 1 - \alpha_t, \quad \forall t \in \mathcal{T}_{CC} \tag{28}$$

Chance constraints introduce a probability that planned electrification will be temporarily delayed. This does introduce a social and economic cost; some will end up waiting longer to receive their desired amount of electricity, even though full electrification will be achieved by the planning period end date. Given that this model is developed in the context of a country that does not yet have a full electricity infrastructure, we do not introduce a new penalty for utilizing the chance constraint. The magnitude of the risk parameter α_t represents the decision-maker's tolerance for slower electrification in the intermediate years. This issue is further discussed with the case study results.

4.2. Linearization of chance constraints

Chance constraint (28) is a probabilistic constraint which is computationally intractable. By taking into account the probabilities of the scenarios and the structure of the scenario tree, the chance constraint (28) can be formulated as a set of mixed-integer linear constraints (29)–(31). We define a binary variable $\lambda_{\omega,t}$ which takes value 1 if the demand satisfaction constraint is violated for scenario ω at year t, and 0 otherwise. The reformulation is represented as follows.

$$\lambda_{\omega,t} \in \{0, 1\}, \quad \forall \omega, t \in \mathcal{T}_{CC} \tag{29}$$

$$\eta_i^{dist} E^{\text{use-C}}_{i,t,o,\omega} \ge D_{i,t,o,\omega}(1 - \lambda_{\omega,t}), \quad \forall i, t \in \mathcal{T}_{CC}, o, \omega \tag{30}$$

$$\sum_{\omega \in \Omega} \pi_\omega \lambda_{\omega,t} \le \alpha_t, \quad \forall t \in \mathcal{T}_{CC} \tag{31}$$

Constraint (30) checks whether the demand is satisfied for all scenarios at those chance-constrained years. The probability of total violations in each year is limited by α_t in constraint (31).

Combining the constraints above, the chance-constrained multi-stage stochastic ESEP model can be formulated into a mixed-integer linear program (MILP) as follows.

min (1)

s.t. (2)–(12), (14)–(25), (26) – (27), (29)–(31)

4.3. Value of chance constraints

It is important to identify the value of the chance-constrained stochastic model as opposed to the non-chance-constrained counterpart. To this end, we define the value of chance constraints in terms of cost and percentage gain in (32) and (33).

$$VCC(\$) = V^{NCC} - V^{CC} \tag{32}$$

$$VCC(\%) = \frac{V^{NCC} - V^{CC}}{V^{NCC}} \times 100 \tag{33}$$

Here, V^{NCC} and V^{CC} are the optimal objective function values obtained from the non-chance-constrained and chance-constrained models. Since the non-chance-constrained model requires immediate demand satisfaction, it guarantees that $V^{NCC} \geq V^{CC}$. Therefore, the value of chance-constrained model VCC is always non-negative with a trade-off for the possibility of not satisfying demand immediately for some periods in certain scenarios. Additionally, the value of chance constraints can be separately computed for different scenarios, which is expected to be higher in large demand scenarios compared to the low demand scenarios and the aggregate model. Note that the impact of the chance-constrained model is beyond the direct costs and benefits, as the model brings a more moderate investment plan over the planning horizon, as analyzed in the case study.

5. Solution heuristic

When the number of scenarios increases in this stochastic problem, the number of variables increases dramatically and the resulting large-scale problem can be computationally intractable. To overcome this difficulty, the problem can be decomposed with respect to scenarios and solved by a Progressive Hedging Algorithm (PHA) [26], as forumlated in Section 5.1. The MILP formulation of the chance-constrained model in Section 4.2 links different scenarios as it has an overall risk parameter for the chance-constrained time periods. To address this issue, we consider a Lagrangian relaxation of the chance-constrained problem and develop a binary-search-based PHA heuristic for its solution in Section 5.2.

5.1. Progressive hedging algorithm

A PHA iteratively solves the individual scenario sub-problem in parallel by relaxing non-anticipativity constraints within a penalty function to force the solution to gradually converge to the overall optimal solution. The algorithm converges when all solutions of the subproblems satisfy the non-anticipativity constraints. In this section, we outline PHA for multi-stage stochastic electrification planning.

We describe the PHA implementation in a compact formulation. Additional notation for the compact formulation are described as follows:

$f_{\omega,t}$: costs associated with state variables at year t under scenario ω.

$\phi_{\omega,t}$: costs associated with stage variables at year t under scenario ω.

$\Delta_{\omega,t}$: set of constraints in (2)–(23) at year t under scenario ω.

$\boldsymbol{x}_{\boldsymbol{\omega},\boldsymbol{t}}$: vector of state variables at year t under scenario ω.

$\boldsymbol{y}_{\boldsymbol{\omega},\boldsymbol{t}}$: vector of stage variables at year t under scenario ω.

The MILP model defined in (1)–(25) can be rewritten in a compact formulation as:

$$\min_{x,y} \quad \sum_{\omega\in\Omega} \pi_\omega [\sum_{t\in\mathcal{T}} (f_{\omega,t}^T \boldsymbol{x}_{\boldsymbol{\omega},\boldsymbol{t}} + \phi_{\omega,t}^T \boldsymbol{y}_{\boldsymbol{\omega},\boldsymbol{t}})] \tag{34}$$

$$\text{s.t.} \quad (\boldsymbol{x}_{\boldsymbol{\omega},\boldsymbol{t-1}}, \boldsymbol{x}_{\boldsymbol{\omega},\boldsymbol{t}}, \boldsymbol{y}_{\boldsymbol{\omega},\boldsymbol{t}}) \in \Delta_{\omega,t}, \quad \forall \omega, t \tag{35}$$

$$\boldsymbol{x}_{\boldsymbol{\omega},\boldsymbol{t}} = \boldsymbol{x}_{\boldsymbol{\omega}',t} \quad \forall (\omega,\omega') \in \Omega_t, t \tag{36}$$

Objective (34) represents the expected total cost for all scenarios and time periods. Constraint (35) includes the constraints for the multi-stage stochastic ESEP process. Non-anticipativity for state variables are constrained in (36), which means all investment decisions shall be the same for all scenarios that are indistinguishable up to that year. The non-anticipativity constraint (36) is the key point for the PHA since it links the scenarios in the optimization problem. By relaxing this constraint, we can decompose the problem with respect to scenarios. Constraint (36) can be reformulated as:

$$\boldsymbol{x}_{\boldsymbol{\omega},\boldsymbol{t}} = \bar{\boldsymbol{x}}_n, \quad \forall n \in \Sigma_t, (\omega,t) \in \Gamma(n), t \in \mathcal{T}, \tag{37}$$

where n denotes a node on the scenario tree, Σ_t is the set of nodes on the scenario tree at year t, and $\Gamma(n)$ denotes the pairs of scenarios and time periods that are considered in node n. When the scenario and year are known, one specific node on the scenario tree shall be identified. To ensure the non-anticipativity constraint, we define $\bar{\boldsymbol{x}}_n$ as the consensus variable for node n of the scenario tree. This value can be updated as

$$\bar{\boldsymbol{x}}_n = \frac{\sum_{(\omega,t)\in\Gamma(n)} \pi_\omega \boldsymbol{x}_{\boldsymbol{\omega},\boldsymbol{t}}}{\sum_{(\omega,t)\in\Gamma(n)} \pi_\omega}, \quad \forall n \tag{38}$$

which calculates the average value of the current state variables at year t under scenario ω. At the optimal solution, all the state variables $\boldsymbol{x}_{\boldsymbol{\omega},\boldsymbol{t}}$ corresponding to node n should be the same as this consensus value $\bar{\boldsymbol{x}}_n$ as in (38).

The augmented Lagrangian problem is based on the relaxation of non-anticipativity constraint (36) and defined as:

$$\min_{x,y,\bar{x}} \quad \sum_{\omega\in\Omega} \pi_\omega L_\omega(\boldsymbol{x}_{\boldsymbol{\omega},\boldsymbol{t}}, \boldsymbol{y}_{\boldsymbol{\omega},\boldsymbol{t}}, \bar{\boldsymbol{x}}_n) \tag{39}$$

$$\text{s.t.} \quad (35) \tag{40}$$

where

$$L_\omega(\boldsymbol{x}_{\boldsymbol{\omega},\boldsymbol{t}}, \boldsymbol{y}_{\boldsymbol{\omega},\boldsymbol{t}}, \bar{\boldsymbol{x}}_n) = \sum_{t\in\mathcal{T}} (f_{\omega,t}^T \boldsymbol{x}_{\boldsymbol{\omega},\boldsymbol{t}} + \phi_{\omega,t}^T \boldsymbol{y}_{\boldsymbol{\omega},\boldsymbol{t}} + \delta_{\omega,t}^T (\boldsymbol{x}_{\boldsymbol{\omega},\boldsymbol{t}} - \bar{\boldsymbol{x}}_n) + \frac{\rho}{2} \left\| \boldsymbol{x}_{\boldsymbol{\omega},\boldsymbol{t}} - \bar{\boldsymbol{x}}_n \right\|_2^2) \tag{41}$$

$L_\omega(\boldsymbol{x}_{\boldsymbol{\omega},\boldsymbol{t}}, \boldsymbol{y}_{\boldsymbol{\omega},\boldsymbol{t}}, \bar{\boldsymbol{x}}_n)$ is the augmented Lagrangian penalty function for each scenario ω. $\delta_{\omega,t}$ is the common Lagrange multiplier and $\rho > 0$ is the penalty parameter. It is easy to observe that the augmented Lagrangian problem defined in (39)–(40) can be solved separately in different scenarios if $\delta_{\omega,t}$ and $\bar{\boldsymbol{x}}_n$ are known in advance. PHA iteratively solves the augmented Lagrangian problem by scenario sub-problems and updates the Lagrange multiplier and the consensus value.

Algorithm 1 describes an overview of PHA for the compact formulation in (34)–(36). The penalty parameter ρ and the convergence tolerance ϵ are the inputs for the algorithm. The iteration counter is v and starts with 0. Line 2 initializes the counter, gap, and Lagrange multiplier. Lines 3–5 find the initial state variables by solving the problem without Lagrangian penalty terms. The main idea of PHA is inside the while loop from line 7 to 13. In each iteration, the algorithm updates the consensus value $\bar{\boldsymbol{x}}_n$ in line 7 and the Lagrange multiplier $\delta_{\omega,t}$ in line 9 by the current state variables. Lines 10–12 solve the augmented Lagrangian problem for each scenario and update the most recent state variables $\boldsymbol{x}_{\boldsymbol{\omega},\boldsymbol{t}}$. The algorithm terminates when all non-anticipativity constraints are satisfied within the convergence tolerance ϵ.

5.2. Binary-search-based PHA heuristic for chance-constrained problem

Expressing the chance-constrained ESEP problem more compactly, we define $\Psi_{\omega,t}$ as the set of constraints (2)–(11), (14)–(23), (26)–(27), and (29)–(30), so that the model can be written as follows:

$$\min_{x,y} \quad \sum_{\omega\in\Omega} \pi_\omega [\sum_{t\in\mathcal{T}} (f_{\omega,t}^T \boldsymbol{x}_{\boldsymbol{\omega},\boldsymbol{t}} + \phi_{\omega,t}^T \boldsymbol{y}_{\boldsymbol{\omega},\boldsymbol{t}})] \tag{42}$$

$$\text{s.t.} \quad (\boldsymbol{x}_{\boldsymbol{\omega},\boldsymbol{t-1}}, \boldsymbol{x}_{\boldsymbol{\omega},\boldsymbol{t}}, \boldsymbol{y}_{\boldsymbol{\omega},\boldsymbol{t}}, \lambda_{\omega,t}) \in \Psi_{\omega,t}, \quad \forall \omega, t \tag{43}$$

$$\boldsymbol{x}_{\boldsymbol{\omega},\boldsymbol{t}} = \boldsymbol{x}_{\boldsymbol{\omega}',t}, \quad \forall (\omega,\omega') \in \Omega_t, t \tag{44}$$

$$\sum_{\omega\in\Omega} \pi_w \lambda_{w,t} \leq \alpha_t, \quad \forall t \in \mathcal{T}_{CC} \tag{45}$$

Algorithm 1 Progressive Hedging Algorithm (PHA)

input: ρ, ϵ
initialization: $v \leftarrow 0$, gap $\leftarrow \infty$, $\delta^0_{\omega,t} \leftarrow \mathbf{0}$ $\forall \omega, t$
for $\omega \in \Omega$ **do**
  $\boldsymbol{x}^{\boldsymbol{v}}_{\boldsymbol{\omega},\boldsymbol{t}} \leftarrow$ argmin $\sum_{t\in\mathcal{T}}(f^T_{\omega,t}\boldsymbol{x}_{\boldsymbol{\omega},\boldsymbol{t}} + \phi^T_{\omega,t}\boldsymbol{y}_{\boldsymbol{\omega},\boldsymbol{t}})$ s.t. (35)
end for
while gap $\geq \epsilon$ **do**
  $\bar{\boldsymbol{x}}^{\boldsymbol{v}}_{\boldsymbol{n}} = \frac{\sum_{(\omega,t)\in\Gamma(n)}\pi_\omega \boldsymbol{x}^{\boldsymbol{v}}_{\boldsymbol{\omega},\boldsymbol{t}}}{\sum_{(\omega,t)\in\Gamma(n)}\pi_\omega}$ $\forall n$
  $v \leftarrow v+1$
  $\delta^v_{\omega,t} \leftarrow \delta^{v-1}_{\omega,t} + \rho(\boldsymbol{x}^{\boldsymbol{v-1}}_{\boldsymbol{\omega},\boldsymbol{t}} - \bar{\boldsymbol{x}}^{\boldsymbol{v-1}}_{\boldsymbol{n}})$ $\forall \omega, t$
  for $\omega \in \Omega$ **do**
    $\boldsymbol{x}^{\boldsymbol{v}}_{\boldsymbol{\omega},\boldsymbol{t}} \leftarrow$ argmin (41) s.t. (35)
  end for
  gap $\leftarrow \sqrt{\sum_{\omega\in\Omega}\sum_{t\in\mathcal{T}}\pi_\omega \|\boldsymbol{x}^{\boldsymbol{v}}_{\boldsymbol{\omega},\boldsymbol{t}} - \bar{\boldsymbol{x}}^{\boldsymbol{v-1}}_{\boldsymbol{n}}\|_2^2}$
end while

All constraints in $\Psi_{\omega,t}$ are separable with respect to scenarios. Constraint (45) is the limitation on total violations for chance constraints at each corresponding year by considering all scenarios. It is easy to observe that the problem with objective function (42) and constraints (43)–(44) is in the same form as in the previous setting without chance constraints, which can be solved by PHA. We express the Lagrangian relaxation of the chance-constrained problem (42)–(45) as follows:

$$\min_{x,y} \sum_{\omega\in\Omega}\pi_\omega[\sum_{t\in\mathcal{T}}(f^T_{\omega,t}\boldsymbol{x}_{\boldsymbol{\omega},\boldsymbol{t}} + \phi^T_{\omega,t}\boldsymbol{y}_{\boldsymbol{\omega},\boldsymbol{t}})] - \sum_{t\in\mathcal{T}_{CC}} w_t \sum_{\omega\in\Omega}(\pi_\omega\lambda_{\omega,t} - \alpha_t) \quad (46)$$

$$\text{s.t.} \quad (\boldsymbol{x}_{\boldsymbol{\omega},\boldsymbol{t-1}}, \boldsymbol{x}_{\boldsymbol{\omega},\boldsymbol{t}}, \boldsymbol{y}_{\boldsymbol{\omega},\boldsymbol{t}}, \lambda_{\omega,t}) \in \Psi_{\omega,t}, \quad \forall \omega, t \quad (47)$$

$$\boldsymbol{x}_{\boldsymbol{\omega},\boldsymbol{t}} = \boldsymbol{x}_{\boldsymbol{\omega}',\boldsymbol{t}}, \quad \forall(\omega,\omega') \in \Omega_t, t \quad (48)$$

where $w_t \geq 0, \forall t \in \mathcal{T}_{CC}$ is the Lagrangian multiplier for constraint (45). If the Lagrangian multiplier w_t is known in advance, the Lagrangian relaxation problem (46)–(48) can be reformulated as for the problem (34)–(36), that can be solved by PHA. To determine the value of the Lagrangian multiplier w_t, we develop a binary-search-based PHA heuristic for solving the chance-constrained problem. The proposed procedure is presented in Algorithm 2.

Algorithm 2: Binary-search-based PHA heuristic.

1: **input:** ϵ
2: **initialization:** $s \leftarrow 0$, $\underline{w_t}^0$, $\overline{w_t}^0$ $\forall t \in \mathcal{T}_{CC}$
3: **while** $\frac{\overline{w_t}^s - \underline{w_t}^s}{\underline{w_t}^s} \geq \epsilon$ **do**
4: Solve problem (46)–(48) with $\underline{w_t}^s$ by PHA and record optimal objective value as $\underline{v}$.
5: Solve problem (46)–(48) with $\overline{w_t}^s$ by PHA and record optimal objective value as $\overline{v}$.
6: **if** $\underline{v} \geq \overline{v}$ **then**
7: $\underline{w_t}^{s+1} \leftarrow \frac{\underline{w_t}^s + \overline{w_t}^s}{2}$ $\forall t \in \mathcal{T}_{CC}$
8: **else**
9: $\overline{w_t}^{s+1} \leftarrow \frac{\underline{w_t}^s + \overline{w_t}^s}{2}$ $\forall t \in \mathcal{T}_{CC}$
10: **end if**
11: $s \leftarrow s+1$
12: **end while**

The heuristic initializes a lower and an upper bound for the Lagrangian multiplier w_t. Lines 4–5 solve the Lagrangian relaxation problem by PHA with the given w_t. Lines 6–10 update the Lagrange multiplier w_t based on comparison between the optimal objective values. This loop repeats until the difference between the upper and lower Lagrange multipliers is within a specific tolerance. The proposed heuristic combines both PHA and binary search algorithms. As both algorithms have been proven to converge, the heuristic is expected to converge as well. However, due to the presence of integer decision variables, the solution obtained from the heuristic may not be the optimal one. To compare the solution from the proposed heuristic against the optimal one, we conduct several numerical experiments, which are presented in Section 7.3.

6. Case study: Data preparation

To demonstrate the proposed framework, we construct a case study of Rwanda.

As of June 2020, Rwanda has a residential electrification rate of 55% and the government targets reaching 100% electrification by 2030 [30]. The country is divided into 30 administrative districts [31]. We consider a 15-year time horizon from 2021 to 2035. 24 representative daily sub-periods are used for representing the daily hours for each year. We use a discount factor of 10% and all costs are in 2020 USD. Two scenario trees, baseline and extreme, are set up for comparison. Each scenario tree considers 9 scenarios with 3 stages over demand possibilities: low, normal, and high annual increase rate at each stage.

From the average Rwandan electricity infrastructure budget [32], we assume a budget limitation of 80 million dollars for new power infrastructure each year. The GHG emissions from the energy sector is about 1.1 million tons of CO2 as of 2018 [33]. We set a GHG emission limitation at 2 million tons from 2021 to 2025 and set 2.1 to 3 million tons GHG emission limitation for the next 10 years with 0.1 million ton increment each year.

6.1. Generation and transmission infrastructure

The current grid-connected generation sources in Rwanda include diesel, hydroelectric (hydro), natural gas, peat, and solar [30]. The case study considers six generation types: diesel, geothermal, hydro, natural gas combined cycle (NGCC), peat, and utility-scale solar. We choose this simplified list of generation options, and model only grid-connected electricity options, in order to illustrate the benefits of our model. The cost data are summarized in Table 1. Fuel costs are projected to increase over the planning horizon and the other costs are modeled as constant. General and location-specific generation costs and parameters are acquired from [20,34], respectively.

Other parameters associated with generation are given in Table 2. All parameters are independent of time and we assume they are the same for all daily sub-periods during the planning horizon. Capacity factors vary by daily sub-period and are adapted from [34]. Construction time is the years needed to build the capacity in the assigned district after the decision of investment. Construction time data are summarized from [20]. The annual minimal and maximal capacity limits are our reasonable estimates. We omit the minimum reserve requirements for simplicity.

For the existing capacity, we use the 25 licensed power plants from the Electricity Report of the Rwanda Utilities Regulatory Authority (RURA) [35]. Due to resource limitations, some generation types are only available in certain regions and some regions can only build power plants up to a certain number of megawatts. We adopt these resource limitations from [34]. We assume diesel and utility-scale solar are widely available in all districts in Rwanda and can be built at any time.

There are three types of transmission lines in Rwanda: 70, 110 and 220 kV lines [30]. To reduce the complexity of the case study, we consider two types of transmission lines: high-voltage (HV) and low-voltage (LV). The costs and other data for transmission lines are provided in Table 3. All the costs are per unit distance and are adapted from [36]. We assume it takes one year to build both high-voltage and low-voltage transmission lines. The model decides whether to build a high-voltage or low-voltage transmission line between adjacent districts. We assume the transmission loss for each line is 10% of the capacity and the distribution efficiency is 90% throughout the country.

Table 1
Case study generation costs.

Generation type	Investment cost ($/kW)	Fixed O&M cost ($/kW)	Variable O&M cost ($/MWh)	Fuel cost ($/MWh)		
				2021–2025	2025–2030	2030–2035
Diesel	1160	22.50	1.88	275	288	300
Geothermal	4090	44.65	3.19	–	–	–
Hydro	2170	47.00	3.36	–	–	–
NGCC	1160	26.32	2.20	71	76	84
Peat	2610	46.33	3.86	29	34	39
Utility-scale solar	1950	30.33	0.25	–	–	–

Table 2
Case study generation parameters.

Generation type	Construction time (years)	GHG emission (ton/MWh)	Annual Construction Limit (MW)	
			Maximal	Minimal
Diesel	0	0.812	20	5
Geothermal	4	–	–	20
Hydro	4	–	–	–
NGCC	3	0.448	–	–
Peat	4	0.996	–	10
Utility-scale solar	1	–	20	5

Table 3
Transmission line data.

	High voltage	Low voltage
Capacity (MW)	100	25
Investment cost ($/km)	150000	15000
O&M cost ($/(MW*km))	15.48	20.65
Construction time (years)	1	1

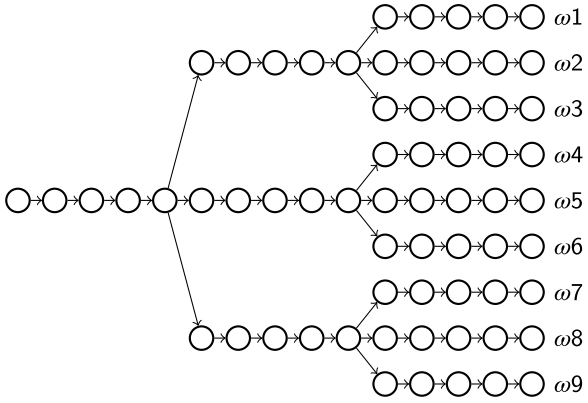

Fig. 3. Scenario tree structure for case study.

6.2. Demand forecast

We consider 24 daily sub-periods for each year, corresponding to daily hours. For simplicity, we ignore the seasonal variability of electricity demand. We forecast the demand via per capita power use similar to [36]. We use the population in the region multiplied by the per-capita power demand to calculate the total power demand in a region. The daily demand profile is adopted from [34]. Electricity demand is the product of the power demand and the total hours in the corresponding daily sub-period.

We model the annual electricity demand increases as tracking the country's GDP increase. Rwanda has averaged a 7% annual GDP increase over the past decade [37]. Therefore, we project 7% annual electricity demand increase for the normal setting.

6.3. Baseline and extreme scenario trees

We consider two scenario trees for comparison: baseline and extreme. Both share the same tree structure but have different demand increase rates. We use the scenario tree structure shown in Fig. 3. The tree has a 15-year planning horizon (2021 to 2035) with 3 time stages and 5 years in each stage. We assume the demand increase rate to remain constant in each time stage for each scenario. There are nine scenarios in total and the middle scenario ($\omega 5$) has a constant 7% annual increase rate in both baseline and extreme scenario trees. The branches represent three demand increase rates: high increase for the upper branch (H), normal increase for the center branch (N), and low increase for the low branch (L). Normal increase rate is 7% for both scenario trees. We assume the probability of having a high or low demand increase rate in each time stage is 10% and having a normal demand increase rate is 80%.

The baseline scenario tree represents the typical expected future scenarios. We use 10% as a high annual demand increase rate (H) and 4% as a low annual demand increase rate (L). Unexpected events such as COVID-19 and local resource development may change the electricity demand dramatically. In order to compare the energy infrastructure development between common scenarios and those unexpected scenarios, we design an extreme scenario tree to represent unforeseen events that strangely influence the demand. The high demand increase rate for the extreme scenario tree is 20% annually and the low increase rate is reduced to 1%. Our goal is to examine the resulting differences between baseline and extreme scenario trees and support countries that use our model in adjusting plans in light of different future scenarios.

6.4. Chance constraints setup

As time progresses over the planning horizon and the scenario tree is further realized, chance constraints provide cost savings by giving the country the opportunity to not fully satisfy the demand in some intermediate years for certain scenarios. In this case study chance constraints are used for the initial two years of each stage of the scenario tree (2026, 2027, 2031, 2032), and to view the impact of these constraints, we assume the risk parameter, α_t, to take the same values for the years in the same stage: $\alpha_{2026} = \alpha_{2027} = \alpha_1$ and $\alpha_{2031} = \alpha_{2032} = \alpha_2$. For 2026 and 2027, since the scenarios in $\omega 1 - \omega 3$ or $\omega 4 - \omega 6$ or $\omega 7 - \omega 9$ keep the same investment decisions, we set the risk tolerance $\alpha_1 = 0.2$. For 2031 and 2032, we allow only one scenario to be violated by setting risk tolerance $\alpha_2 = 0.04$. In the chance-constrained years, we use a minimum demand satisfaction requirement of 70%. We note that the chance constraints are for those four years only, and the model still keeps fully satisfying demand in other years for every scenario. For example, even with the chance constraints, all demands will be satisfied at the last year of the planning horizon (2035).

Table 4
Costs and VCC for baseline and extreme scenario trees. NCC: non-chance-constrained model. CC: chance-constrained model. VCC: value of chance constraints.

	Baseline				Extreme			
	$\omega 1$	$\omega 2$	$\omega 3$	Total	$\omega 1$	$\omega 2$	$\omega 3$	Total
NCC (B$)	4.01	3.74	3.49	3.42	8.06	4.97	4.53	3.82
CC (B$)	3.82	3.61	3.41	3.37	7.66	4.79	4.41	3.75
VCC (B$)	0.19	0.13	0.08	0.05	0.4	0.18	0.12	0.07
VCC (%)	4.74	3.48	2.29	1.46	4.96	3.62	2.65	1.83

7. Case study: Results

The results of our case study in Rwanda are shown and analyzed in this section. We present the benefits of the chance-constrained multi-stage ESEP model in Section 7.1 by demonstrating the cost reduction, cost and capacity mixes, transmission investment, and GHG emissions. We evaluate the impacts of the chance constraint risk parameters and the number of chance-constrained years in Section 7.2. Finally, we analyze the computation times of solving the full model and the model decomposed by the proposed heuristic in Section 7.3. In our case study, the optimization problem consists of $2,103,435$ variables and $3,647,010$ constraints. All studies are implemented in Python and all optimization problems are solved by Gurobi version 9.1.0 on a 2.3 GHz Intel Core i7 processor with 16 GB of memory.

7.1. Chance-constrained model results

By the selection of chance constraint risk parameters, the demand can only be unmet in the largest three demand scenarios ($\omega 1 - \omega 3$) at chance-constrained years for both baseline and extreme scenario trees. As the differences between the optimal solutions of the other six scenarios are relatively smaller, we omit their discussion and focus on analyzing these three scenarios along with the overall model results.

7.1.1. Optimal costs and VCC

Table 4 shows the optimal expected objective costs over all scenarios and the costs of the largest three demand scenarios ($\omega 1 - \omega 3$) for both scenario trees. The optimal total expected cost from the chance-constrained model is 3.37 billion dollars for the baseline scenario tree and 3.75 billion dollars for the extreme scenario tree, with a 1.46% and 1.83% overall reduction compared to the corresponding models without chance constraints, respectively. Furthermore, the values of chance constraints for the first three scenarios are higher than for the models as a whole. The total cost savings in the baseline scenario tree are 4.74%, 3.48%, and 2.29% for scenarios $\omega 1 - \omega 3$ and these numbers become 4.96%, 3.62%, and 2.65% for the extreme scenario tree. This shows up to 4.96% lower cost in building the power infrastructures and providing electricity, when a high demand scenario occurs, since chance constraints provide flexibility in investment plans, supporting countries in managing tight budgets in the ESEP process.

The chance-constrained model provides cost savings by relaxing the pace of electrification in chance-constrained years. That is, for programs with a goal of full electrification by the end year, in a chance constrained year the pace of electrification can be slower; the end requirement for full electrification remains. Table 5 summarizes the unsatisfied scenarios for chance-constrained years and the average percentage of unmet demand over unsatisfied scenarios and all scenarios.

The case study sets the risk parameters α_1 and α_2 to ensure that at most three scenarios may be unsatisfied in 2026 and 2027 and one scenario may be unsatisfied in 2031 and 2032, which are the ones with highest demand. In 2026 and 2027, since the first three scenarios share the same electrification increase rate, the unsatisfied scenarios are $\omega 1 - \omega 3$. As $\omega 1$ is the largest demand scenario for 2031 and 2032, it becomes the unsatisfied scenario in those years. Since the case study requires a minimal of 70% satisfaction of the demand in all chance-constrained years, the average unmet electrification percentages in the unmet scenarios are below 30%. Results in Table 5 show the average unmet electrification percentages in unmet scenarios are lower for 2026 and 2027 compared to the years of 2031 and 2032. However, 2026 and 2027 have higher average unmet electrification percentage in all scenarios because there are three failing scenarios compared to one scenario in 2031 and 2032. The extreme scenario tree has a slightly larger average unmet electrification percentage, due to its high demand.

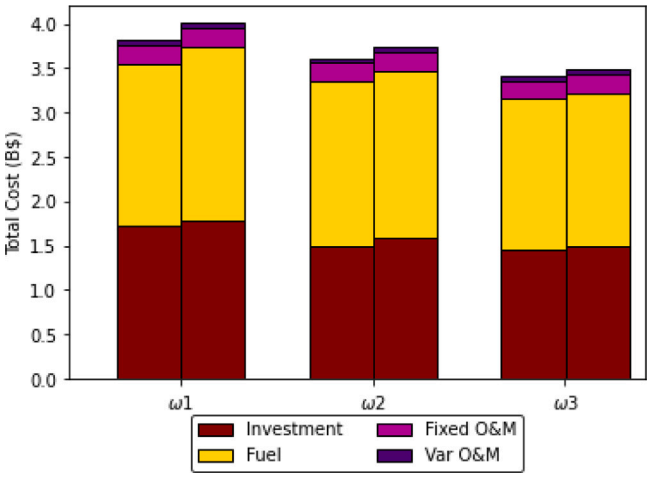

Fig. 4. Total cost mix for the baseline scenario tree. The left-hand bar is the chance-constrained model result; the right-hand bar is the non-chance-constrained model result.

In this model, the societal and economic costs of unmet demand are external, as are opportunities to increase the budget or to exercise demand management on the customer base [38]. The information in Table 4 and Table 5, quantifying the savings and the unmet demand, provides decision-makers with information that could be used to evaluate not only the savings, but also to develop demand management options.

7.1.2. Total cost and capacity mix

Cost mixes for the first three scenarios are shown in Fig. 4 and Fig. 5 for the baseline and extreme scenario trees. Total cost decreases from scenario $\omega 1$ to $\omega 3$ as the demand decreases. The largest components of the cost are investment and fuel costs. The chance-constrained model has smaller investment and fuel costs in all three scenarios for both scenario trees. The difference in total cost between the chance-constrained and non-chance-constrained models becomes smaller from scenario $\omega 1$ to $\omega 3$. The total cost differs more between scenarios for the extreme scenario tree.

Fig. 6 and Fig. 7 show the total capacity levels in the first three scenarios for different power technologies at the end of the planning horizon. The most invested power sources are peat and natural gas (NGCC). Corresponding to the lower cost, the chance-constrained model has smaller total capacity built at the end, although all demands are satisfied. We observe that utility-scale solar capacity is higher in chance-constrained model while peat and diesel capacities are higher in the non-chance-constrained model.

Table 5
Unmet scenarios and demand from chance-constrained model in baseline and extreme scenario trees.

Chance-constrained years	Unsatisfied scenarios	Average unmet demand in unsatisfied scenarios (%)		Average unmet demand in all scenarios (%)	
		Baseline	Extreme	Baseline	Extreme
2026	$\omega 1 - \omega 3$	24.7	27.8	4.94	5.56
2027	$\omega 1 - \omega 3$	26.2	29.2	5.24	5.84
2031	$\omega 1$	29.5	29.4	1.18	1.18
2032	$\omega 1$	29.5	29.8	1.18	1.19

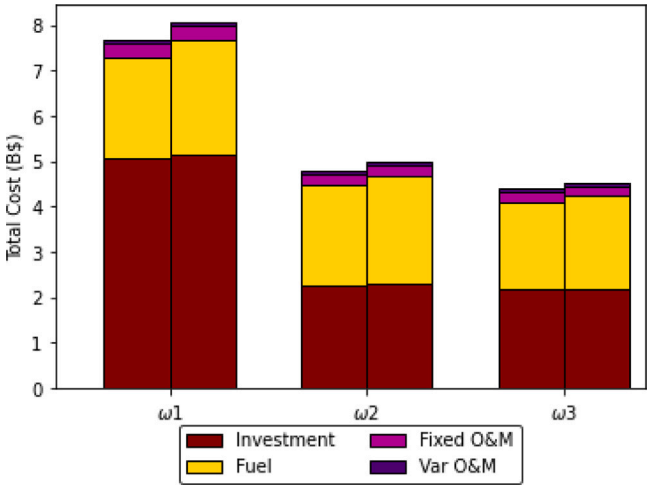

Fig. 5. Total cost mix for the extreme scenario tree. The left-hand bar is the chance-constrained model result; the right-hand bar is the non-chance-constrained model result.

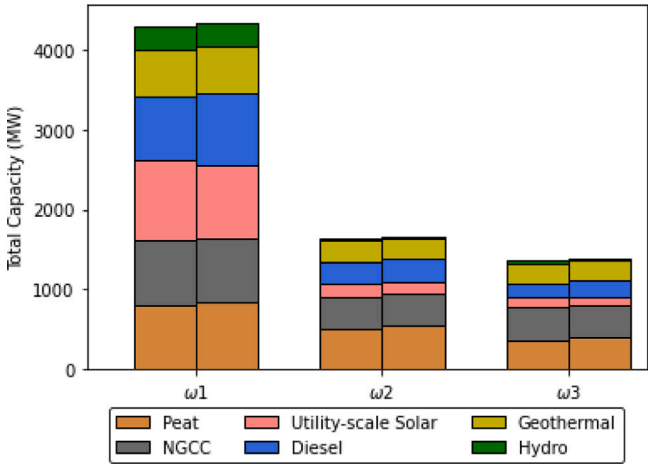

Fig. 7. Capacity mix for the extreme scenario tree. The left-hand bar is the chance-constrained model result; the right-hand bar is the non-chance-constrained model result.

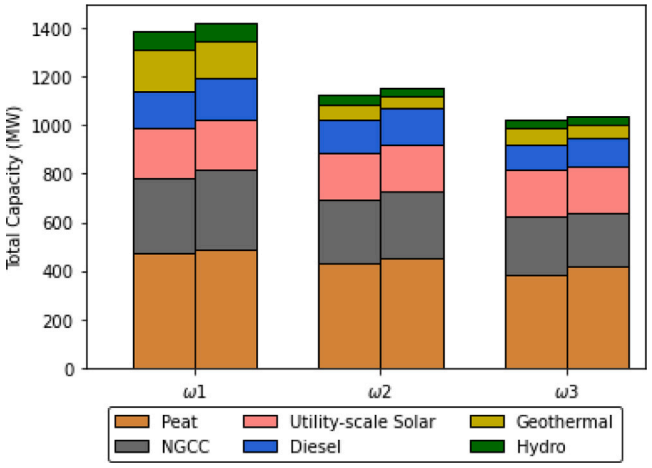

Fig. 6. Capacity mix for the baseline scenario tree. The left-hand bar is the chance-constrained model result, the right-hand bar is the non-chance-constrained model result.

7.1.3. Transmission lines

Table 6 shows that more transmission lines are built in the chance-constrained model than in the non-chance-constrained model, in the first three scenarios. In the baseline scenarios, the chance-constrained result has two more HV transmission lines compared to the non-chance-constrained result. For the extreme scenarios, the chance-constrained result has more HV and LV transmission lines for all three scenarios. As building more transmission lines enables the whole energy system network to be more connected, the chance-constrained model may help countries like Rwanda in balancing the benefits of somewhat slower energy system development, generating a richer transmission network with lower total cost. Without the chance constraints, the model would select generation options that can be built fast; such as diesel generators. With the chance constraints, the model allows the choice of a slower-to-build options, which might include larger natural gas combined cycle generators, or utility scale solar. By loosening the time constraints, planners and the model have more options.

7.1.4. GHG emissions

Yearly GHG emissions from the two models in the first scenario ($\omega 1$) are presented in Fig. 8 (baseline) and Fig. 9 (extreme). GHG emissions are similar for both models in the first 5 years from 2021 to 2026 as the demand levels are the same. In chance-constrained years (2026, 2027, 2031, 2032), the chance-constrained result has a significantly lower GHG emission since it does not require satisfying the demand immediately. After the chance-constrained years, the GHG emission from the chance-constrained result starts to increase but the emission is still slightly lower than the non-chance-constrained models. The lower GHG emissions at chance-constrained years from the chance-constrained model is due to the more solar power capacity as shown in Section 7.1.2. In the end, however, the systems are approximately equal in terms of the yearly GHG emission.

7.2. Impact of the chance constraint parameters

In this section, we first analyze the sensitivity of the optimal total expected cost to different values of chance constraint risk parameters α_1 and α_2. We set α_1 = 0%, 20% and 32% for the years 2026 and 2027, and set α_2 values to 0%, 4%, 20% and 32% for 2031 and 2032. Fig. 10 and Fig. 11 illustrate the optimal total expected cost decrease percentage compared with the non-chance-constrained model. As α_1 increases, the total expected cost decreases. The difference between α_1 = 0 and α_1 = 20% is larger than the difference between α_1 = 20% and α_1 = 32%. With fixed α_1, the optimal total expected cost has a

Table 6
Number of new high (HV) and low (LV) voltage transmission lines constructed in baseline and extreme scenarios.

	Scenario	Baseline		Extreme	
		HV	LV	HV	LV
Chance-constrained	$\omega 1$	34	23	41	22
	$\omega 2$	34	23	40	20
	$\omega 3$	34	23	39	19
Non-chance-constrained	$\omega 1$	32	23	37	19
	$\omega 2$	32	23	37	19
	$\omega 3$	32	23	37	19

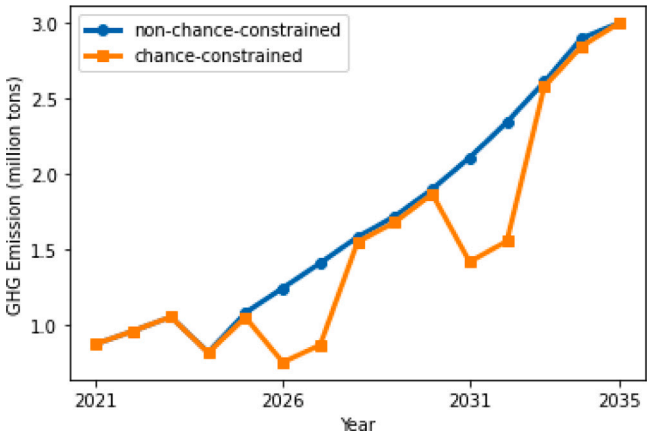

Fig. 8. Yearly GHG emissions in scenario $\omega 1$ for the baseline scenario tree.

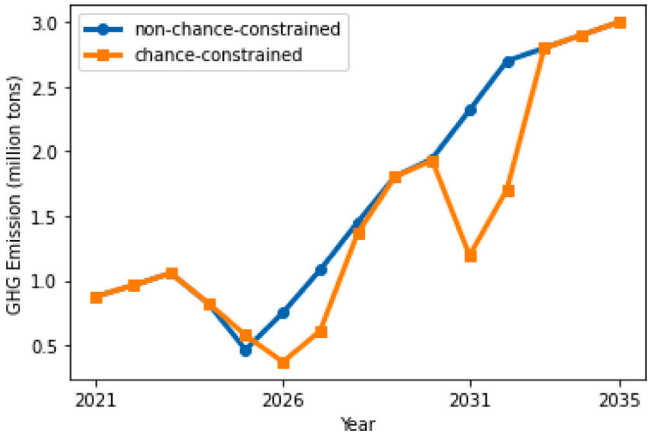

Fig. 9. Yearly GHG emissions in scenario $\omega 1$ for the extreme scenario tree.

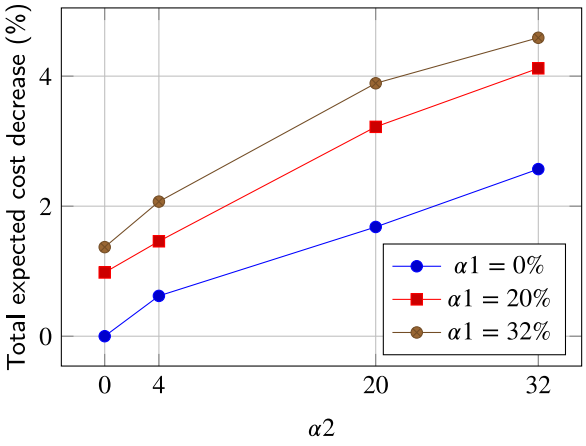

Fig. 10. Optimal total expected cost decrease by different risk parameters for the baseline scenario tree.

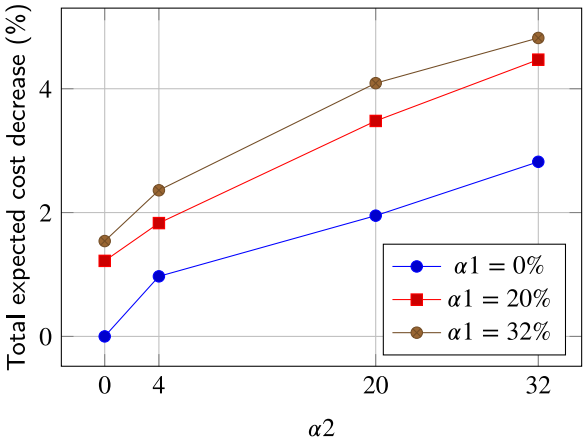

Fig. 11. Optimal total expected cost decrease by different risk parameters for the extreme scenario tree.

larger decrease when α_2 increases for both scenario trees. For $\alpha_1 = 0$ case, the decreases are similar in both scenario trees. For the $\alpha_1 = 20\%$ and $\alpha_1 = 32\%$ cases, the extreme scenario tree decreases a little more. The result shows that the larger α_1 and α_2 values are, the lower the optimal cost is, and more scenarios have unsatisfied demand in the chance-constrained years.

Next, we examine the impact of the number of chance-constrained years. In the case study, we consider four chance-constrained years (two on the second and two on the third time stages). We test the model with four different ranges of chance-constrained years from two to eight years (one to four years on both the second and third time stages). For example, if the total number of chance-constrained years is 6, it means the chance-constrained years are 3 years from 2026 and 3 years from 2031. We still guarantee all demands are met at the end of the planning horizon. Fig. 12 shows the values of chance constraints with different chance-constrained years. As the number of chance-constrained years increases, the chance-constrained model saves more money. The increases of the value of chance constraints (decreases of the total expected cost) in Fig. 12 are supra-linear. The extreme scenario tree has slightly higher value of chance constraint compared to the baseline scenario tree.

7.3. Performance of proposed heuristic

We use PHA as a scenario decomposition tool to achieve better computational performance. In this section, we test the computational performance of the binary-search-based PHA heuristic and the quality of the solutions obtained. We set the Lagrangian penalty parameter ρ as 0.8 and the convergence tolerance ϵ as 0.001. The lower and upper

Table 7
Performance of the proposed heuristic.

		Baseline	Extreme
Directly solve	CPU time (s)	832	1295
	Solution (B$)	3.42	3.82
Heuristicimplementation	CPU time (s)	408	778
	Solution (B$)	3.44	3.85
	Gap (%)	0.58	0.78

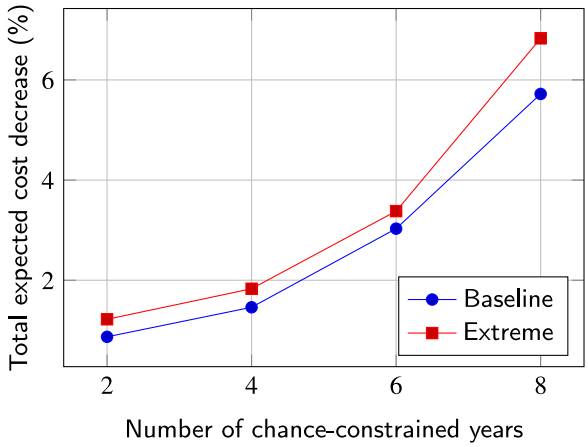

Fig. 12. Optimal total expected cost decrease by different numbers of chance-constrained years.

bounds of the Lagrangian multipliers w_t and $\overline{w_t}$ in the binary search heuristic are initialized as the optimal cost for the lowest demand scenario and the cost obtained by implementing the largest possible infrastructures, respectively. The termination condition for the binary search heuristic is set to be satisfied when the percentage difference between w_t and $\overline{w_t}$ is less than or equal to 0.1%.

Table 7 compares the performance of the direct and heuristic solution approaches for our case study. As expected, for both baseline and extreme scenario trees, the heuristic is faster than solving directly. The heuristic has a gap within 1% of the optimal solution for both scenario trees. The computation times are shorter for the baseline compared with the extreme. The optimality gap is larger for the extreme scenario tree.

Since PHA is a scenario decomposition method, we examine the effects of the proposed heuristic over different numbers of scenarios. We construct six scenario trees with different number of branches (2, 3 or 4) in each stage and different number of time stages (3, 4, or 5). In the 2-branch setting, we consider a 4% and 10% annual demand increase rate. In the 3-branch setting, we keep annual increase the same as our baseline scenario tree (4%, 7%, and 10%). In the 4-branch setting, the annual demand increase rates are set as 4%, 6%, 8%, and 10%. For the 3-stage case, we have 5 years in each stage. For the 4-stage case, we have 3, 4, 4, and 4 years in each time stage, and we split to 3 years in each stage for the 5-stage case. We stop running the algorithm if the run time exceeds 3600s.

The performance results, summarized in Table 8, show the heuristic is faster for most scenario trees except when there are only 4 scenarios (2 branches and 3 stages). Results have fairly small optimally gap (less than 1.33%) in all scenario trees. The optimality gap increases as the number of scenarios increases. The results demonstrate that the binary-search-based PHA heuristic has computational advantage in cases with a large number of scenarios. The heuristic may not be necessary if the number of scenarios is small, particularly as multi-year ESEP modeling may not have highly constrained computational time requirements. The heuristic approach can be beneficial for large-scale applications in which the direct approach does not find the optimal solution in a reasonable amount of time. As we have shown, both the direct solution approach and the heuristic provide viable solutions.

Different choice of penalty parameter, and application to different problems, will affect convergence and computation time. Comparing the baseline and extreme cases in Table 7, we see that the PHA performance is somewhat better in the baseline than in the extreme scenario. To expedite the computation time of PHA, various enhancements can be implemented, including adjusting penalty parameters [39], linearizing quadratic penalty terms [40], improving termination criteria, and other related approaches [41]. These works provide methods for choosing the penalty parameter and reducing computation time.

8. Conclusion

The chance-constrained multi-stage stochastic ESEP model established in this paper addresses the challenge of high future electricity demand uncertainty in the energy system planning process. By considering both investment and operational constraints for power infrastructures, the model provides decision makers with a valuable tool to revise investment decisions annually, adapting to the actual demand realization. One of the key advantages of the proposed model is its incorporation of chance constraints, which allow for the possibility of lower supply than demand in chance-constrained years. This flexibility helps reduce the overall expected cost and also mitigates the costs associated with unexpectedly high demand scenarios.

The numerical test for the country of Rwanda involves two scenario trees: baseline and extreme. From an expected annual demand increase of 7%, the baseline scenario tree considers annual demand increases ranging from a low of 4% to a high of 10%. The extreme scenario tree considers annual demand increases ranging from 1% to 20%. The values of chance constraints are 1.46% and 1.83% for the baseline and extreme scenario trees respectively, compared to a non-chance-constrained model. The values of chance constraints increase to 4.74% and 4.96% when considering the largest demand scenario. Other benefits of implementing chance constraints include potential improvements in transmission infrastructure through the construction of more transmission lines, and the ability to achieve a lower-cost system with policy constraints such as greenhouse gas (GHG) emission reduction.

The implementation of chance constraints presents a trade-off between cost reductions and the extent and duration of unmet demand. By adjusting the risk parameter and the length of the chance-constrained period, the overall cost can be lowered, but this comes at the expense of delaying the fulfillment of demand. The larger the risk parameter, the lower the overall cost, although with the consequent delay in meeting the demand. As the risk parameter values (α_1, α_2) approach to $(32\%, 32\%)$, the model for the extreme scenario tree has an almost 5% optimal total expected cost reduction. Similarly, the longer the chance-constrained length, the more the model saves. When the number of chance-constrained years is eight years, the model has a value of chance constraints of more than 6%. These findings highlight the importance of carefully selecting risk parameters and determining the duration of chance constraints. By appropriately adjusting these parameters, decision-makers can strike a balance between cost reduction and meeting demand requirements within specified timeframes.

The results of the numerical tests indicate that the proposed PHA heuristic requires less computational time compared to direct solution,

Table 8
Performance of the proposed heuristic with different number of scenarios.

(# branches, # time stages)	# scenarios	Directly solve		PHA		
		Cost (B$)	CPU Time (s)	PH Cost (B$)	CPU Time (s)	Gap (%)
(2, 3)	4	3.195	166	3.196	183	0.03
(2, 4)	8	3.236	357	3.243	292	0.22
(2, 5)	16	3.293	539	3.304	322	0.33
(3, 3)	9	3.423	832	3.443	408	0.58
(3, 4)	27	3.512	1255	3.540	781	0.79
(3, 5)	81	3.748	2834	3.793	1977	1.20
(4, 3)	16	3.915	966	3.944	525	0.74
(4, 4)	64	4.133	2520	4.177	1734	1.06
(4, 5)	256	4.216	3600	4.272	3291	1.33

with relatively small gap between the heuristic and optimal solution. This computational advantage is particularly significant in cases with a large number of scenarios.

Our work suggests several future research directions. The multi-stage stochastic model requires the decision-maker to adapt to the uncertainty in each time stage by adjusting the investment plan. This may not be operationally feasible. A partially flexible stochastic model that combines the best features of two-stage and multi-stage stochastic optimization is appealing and could be developed. Additionally, other risk reduction methods such as risk-averse objectives can be evaluated and compared.

CRediT authorship contribution statement

Yuang Chen: Conceptualization, Methodology, Investigation, Software, Data curation, Visualization, Writing – original draft. **Beste Basciftci:** Conceptualization, Investigation, Methodology, Validation, Writing – review & editing. **Valerie M. Thomas:** Data curation, Validation, Writing – review and editing.

Declaration of competing interest

The authors declare that they have no known competing financial interests or personal relationships that could have appeared to influence the work reported in this paper.

Data availability

Data will be made available on request.

Acknowledgment

This research was partially supported by the Shenzhen Science and Technology Innovation Commission's 2022 University Stable Support Program.

References

[1] Riva F, Ahlborg H, Hartvigsson E, Pachauri S, Colombo E. Electricity access and rural development: Review of complex socio-economic dynamics and causal diagrams for more appropriate energy modelling. Energy Sustain Dev 2018;43:203–23.
[2] Seddighi AH, Ahmadi-Javid A. Integrated multiperiod power generation and transmission expansion planning with sustainability aspects in a stochastic environment. Energy 2015;86:9–18.
[3] Boait P, Advani V, Gammon R. Estimation of demand diversity and daily demand profile for off-grid electrification in developing countries. Energy Sustain Dev 2015;29:135–41.
[4] Kenya Power. Report of the presidential task force on the review of power purchase agreements. 2021, <https://kplc.co.ke/img/full/28102021_210-The-Report-of-the-Presidential-Taskforce-on-PPAs.pdf> Accessed: 2022-06-19.
[5] Fobi S, Deshpande V, Ondiek S, Modi V, Taneja J. A longitudinal study of electricity consumption growth in Kenya. Energy Policy 2018;123:569–78.
[6] Sekanabo D, Nyandwi E, J.K. H, Thomas VM. The relationship between GDP and biomass energy per capita in Sub-Saharan Africa. Int J Energy Econ Policy 2022;12(3):151–60.
[7] Huang Y-H, Wu J-H, Hsu Y-J. Two-stage stochastic programming model for the regional-scale electricity planning under demand uncertainty. Energy 2016;116:1145–57.
[8] Conejo AJ, Baringo L, Kazempour SJ, Siddiqui AS. Investment in electricity generation and transmission, Vol. 106. Cham Zug, Switzerland: Springer International Publishing, Springer; 2016.
[9] Zhou Z, Zhang J, Liu P, Li Z, Georgiadis MC, Pistikopoulos EN. A two-stage stochastic programming model for the optimal design of distributed energy systems. Appl Energy 2013;103:135–44.
[10] Pereira MV, Pinto LM. Multi-stage stochastic optimization applied to energy planning. Math Program 1991;52(1):359–75.
[11] Go RS, Munoz FD, Watson J-P. Assessing the economic value of co-optimized grid-scale energy storage investments in supporting high renewable portfolio standards. Appl Energy 2016;183:902–13.
[12] Jenabi M, Ghomi SMTF, Smeers Y. Bi-level game approaches for coordination of generation and transmission expansion planning within a market environment. IEEE Trans Power syst 2013;28(3):2639–50.
[13] Roldán C, de la Nieta AS, García-Bertrand R, Mínguez R. Robust dynamic transmission and renewable generation expansion planning: walking towards sustainable systems. Int J Electr Power Energy Syst 2018;96:52–63.
[14] Peker M, Kocaman AS, Kara BY. A two-stage stochastic programming approach for reliability constrained power system expansion planning. Int J Electr Power Energy Syst 2018;103:458–69.
[15] Pantoš M. Stochastic generation-expansion planning and diversification of energy transmission paths. Electr Power Syst Res 2013;98:1–10.
[16] Baringo L, Conejo AJ. Transmission and wind power investment. IEEE Trans Power Syst 2012;27(2):885–93.
[17] Guerra OJ, Tejada DA, Reklaitis GV. An optimization framework for the integrated planning of generation and transmission expansion in interconnected power systems. Appl Energy 2016;170:1–21.
[18] Georgiou PN. A bottom-up optimization model for the long-term energy planning of the greek power supply sector integrating mainland and insular electric systems. Comput Oper Res 2016;66:292–312.
[19] Guo Z, Cheng R, Xu Z, Liu P, Wang Z, Li Z, et al. A multi-region load dispatch model for the long-term optimum planning of China's electricity sector. Appl Energy 2017;185:556–72.
[20] Ioannou A, Fuzuli G, Brennan F, Yudha SW, Angus A. Multi-stage stochastic optimization framework for power generation system planning integrating hybrid uncertainty modelling. Energy Econ 2019;80:760–76.
[21] Chen Y, Basciftci B, Thomas VM. Multi-stage stochastic electrification planning under demand uncertainty. In: 2022 IEEE PES/IAS PowerAfrica. 2022, p. 1–5.
[22] Charnes A, Cooper WW. Chance-constrained programming. Manage Sci 1959;6(1):73–9.
[23] Huang G, Niu Y, Lin Q, Zhang X, Yang Y. An interval-parameter chance-constraint mixed-integer programming for energy systems planning under uncertainty. Energy Sources, Part B: Econ, Plan, Policy 2011;6(2):192–205.
[24] Zhou X, Huang G, Zhu H, Chen J, Xu J. Chance-constrained two-stage fractional optimization for planning regional energy systems in British Columbia, Canada. Appl Energy 2015;154:663–77.
[25] Shapiro A, Dentcheva D, Ruszczynski A. Lectures on stochastic programming: Modeling and theory. SIAM; 2021.
[26] Rockafellar RT, Wets RJ-B. Scenarios and policy aggregation in optimization under uncertainty. Math Oper Res 1991;16(1):119–47.
[27] Maluenda B, Negrete-Pincetic M, Olivares DE, Lorca Á. Expansion planning under uncertainty for hydrothermal systems with variable resources. Int J Electr Power Energy Syst 2018;103:644–51.
[28] Gul S, Denton BT, Fowler JW. A progressive hedging approach for surgery planning under uncertainty. INFORMS J Comput 2015;27(4):755–72.
[29] Hu S, Han C, Dong ZS, Meng L. A multi-stage stochastic programming model for relief distribution considering the state of road network. Transp Res B 2019;123:64–87.
[30] Bimenyimana S, Asemota GN, Li L. The state of the power sector in Rwanda: A progressive sector with ambitious targets. Front Energy Res 2018;6:68.

[31] Center for International Earth Science Information Network - CIESIN - Columbia University. Gridded population of the world, version 4 (GPWv4): Administrative unit center points with population estimates, revision 11. 2018, http://dx.doi.org/10.7927/H4BC3WMT.
[32] Ntirenganya E. Rwanda: budget - energy sector faces 90% deficit. 2021, <https://allafrica.com/stories/202105180096.html> Accessed: 2021-10-16.
[33] USEnergy Information Administration. International Energy Statistics: Total Carbon Dioxide Emissions from the Consumption of Energy. 2018, <https://www.eia.gov/international/data> Accessed: 2021-10-16.
[34] Musselman A, Thomas VM, Nazzal D, Papageorgiou DJ, Venkatesh A, Mallapragada DS. The impact of development priorities on power system expansion planning in sub-Saharan Africa. Energy Syst 2021;1–32.
[35] (RURA) RURA. Key statistics in electricity sub-sector. 2019.
[36] Levin T, Thomas VM. A mixed-integer optimization model for electricity infrastructure development. Energy Syst 2013;4(1):79–98.
[37] National Institute of Statistics of Rwanda (NISR). Rwanda statistical yearbook. 2020.
[38] Anjo J, Neves D, Silva C, Shivakumar A, Howells M. Modeling the long-term impact of demand response in energy planning: The Portuguese electric system case study. Energy 2018;165:456–68.
[39] Zehtabian S, Bastin F. Penalty parameter update strategies in progressive hedging algorithm. CIRRELT; 2016.
[40] Helseth A. Stochastic network constrained hydro-thermal scheduling using a linearized progressive hedging algorithm. Energy Syst 2016;7(4):585–600.
[41] Watson J-P, Woodruff DL. Progressive hedging innovations for a class of stochastic mixed-integer resource allocation problems. Comput Manag Sci 2011;8(4):355–70.